CrossMark

Free Convection in a Square Cavity Filled with a Tridisperse Porous Medium

Mohammad Ghalambaz[1] (iD) · **Hossein Hendizadeh**[1] ·
Hossein Zargartalebi[2] · **Ioan Pop**[3]

Abstract This work is dealing with the natural convection heat transfer in a square filled with porous medium that has been extended according to the Nield and Kuznetsov model to tridisperse porous medium. Considering impermeable walls which the horizontal ones are insulated and vertical ones are assumed to be isothermal, the governing equations are set as the three equations for momentum and three equations for energy for three phases of porosity and are numerically solved utilizing finite element method. In this study isothermal contours, streamlines and Nusselt number values are foremost criteria which are presented for three levels of porosity. The influence of various governing parameters on the heat transfer is investigated.

Keywords Free convection · Tridisperse porous media · Boussinesq approximation ·
Paper-type research paper

List of symbols

Latin symbols

d	characteristic length scale
g	gravity
H_1, H_2	dimensionless inter-phase heat transfer parameters.
h_{12}, h_{23}	inter-phase heat transfer coefficients (incorporating specific area)
k_1, k_2, k_3	effective thermal conductivities of the 1-phase, 2-phase and 3-phase

✉ Mohammad Ghalambaz
   m.ghalambaz@iaud.ac.ir

[1] Department of Mechanical Engineering, Dezful Branch, Islamic Azad University, Dezful, Iran

[2] Department of Mechanical Engineering, Shahid Chamran University of Ahvaz, Ahvaz, Iran

[3] Department of Applied Mathematics, Babeş-Bolyai University, 400084 Cluj-Napoca, Romania

🌲 Springer

K	effective permeability of the porous medium
K_{r1}, K_{r2}	permeability ratio
Nu	local Nusselt number
P	excess pressure
Ra	Rayleigh number (based on properties in the 1-phase)
T_1, T_2, T_3	volume-average temperatures of the 1-phase, 2-phase and 3-phase
T_f	volume average of the temperature over the fluid
T_h, T_c	wall temperatures
u_1, u_2, u_3	x-velocity components in the 1-phase, 2-phase, 3-phase
v_1, v_2, v_3	y-velocity components in the 1-phase, 2-phase, 3-phase
x, y	Cartesian coordinates (x-axis is aligned vertically upward, plate is at $y = 0$)

Greek symbol

β_1, β_2	modified thermal diffusivity ratio
β	volumetric thermal expansion coefficient of the fluid
$\gamma_1, \gamma_2, \gamma_3$	modified thermal conductivities
ζ_{12}	velocity coupling coefficient for momentum transfer between phases 1 and 2 (between macro- and meso-pores)
ζ_{23}	velocity coupling coefficient for momentum transfer between phases 2 and 3 (between meso- and micro-pores)
θ	dimensionless temperatures
μ	dynamic viscosity of the fluid
ρ_c	heat capacity per unit volume of the fluid
ρ_f	density of the fluid
σ_1, σ_2	inter-phase momentum transfer parameters
τ_1, τ_2	volume fractions
ϕ_1	macro-porosity
ϕ_2	meso-porosity
ϕ_3	micro-porosity
ψ_1, ψ_2, ψ_3	stream functions for the 1-phase, 2-phase, 3-phase

1 Introduction

The natural convection heat transfer in a cavity at different boundary conditions is one of the most important classical problems (Cheng 2015). Also an enclosure heated from a side is the most significant case in porous systems that shows many useful results at many different applications, such as thermal energy technology, petroleum reservoir, geothermal energy utilization, pollutant dispersion in aquifers, food industry and the insulation for building. In this regard, the fundamental nature and the growing volume of work are sufficiently documented in books by Nield and Bejan (2013), Pop and Ingham (2001), Vafai (2005), Bejan et al. (2004), Ingham and Pop (2005), De Lemos (2012) and Vadasz (2008). Moreover, the case of cavity filled with a porous medium also has many types and levels. We mention also the papers by Sheremet and Pop (2014a, b), Sheremet and Grosan (2015) and Ghalambaz et al. (2015) on free convection in porous cavities filled with a nanofluid. In addition, the paper by Nield and Kuznetsov (2015) on the effect of vertical throughflow on thermal instability

in a porous medium layer saturated by a nanofluid could be of great interest for researchers working on nanofluid problems.

Chen et al. (2000a) implemented a theoretical and experimental study in which the stagnant thermal conductivity of bidisperse porous media considering various micro- and macro-porosities was measured. Chen et al. (2000a) conducted an experimental study of two-phase flow and boiling heat transfer in a channel which is packed with sintered copper bidisperse porous medium. They found that the effective two-phase heat sink of bidispersed porous materials is higher than monodispersed one with the same pore diameter as the micro-pore diameter of the bidispersed porous material. Nield and Kuznetsov (2004) studied the conjugate problem considering forced convection in a bidispersed local thermal nonequilibrium porous medium channel. The case of square cavity for bidisperse porous medium has been studied by Revnic et al. (2009) that contains two levels of porosity, i.e., the macro-porosity which relates to macro-pores and the meso-porosity in which the solid phase of the standard porous medium is replaced by another porous medium. Comparing the influences of a modified thermal capacity ratio parameter, the fluid phase momentum transfer parameter, permeability ratio parameter, modified thermal conductivity ratio parameter and inter-phase heat transfer parameter H on the heat and mass transfer, it is concluded that the inter-phase heat transfer parameter and the modified thermal conductivity ratio have much more impact on transport phenomena with respect to other mentioned parameters (Revnic et al. 2009). Nield and Kuznetsov (2011) have considered extended bidisperse porous medium (BDPM) to the case of three levels of porosity or namely tridisperse porous medium (TDPM) for a heated vertical wall embedded in tridisperse porous medium. According to Nield and Kuznetsov research, level 1 is macro-porosity, level 2 is meso-porosity and level 3 is micro-porosity and they found a similarity solution based on the characteristics of TDPM. They also on the other investigation formulated a three-velocity three-temperature model for tridisperse porous media and obtained an analytical solution (Nield and Kuznetsov 2011a). Kuznetsov and Nield (2011) resolved the classical Rayleigh–Benard problem for the onset of convection in a horizontal layer which is uniformly heated from bottom in a tridisperse porous medium.

The natural heat transfer in a square filled with regular porous medium with constant temperature applied for vertical walls and remaining two horizontal walls at adiabatic constraint has been studied by many authors, Bejan (1979), Baytas and Pop (2001) and the extended case for a BDPM investigated by Revnic et al. (2009). In this paper the governing relations considered as three continuity, three momentum (Darcy model) and three energy equations for three levels of porosity and after simplifying and nondimensionalizing relations, the final governing partial differential equations are numerically solved for a cavity using the finite element method. Moreover, the effect of important parameters on the flow and temperature fields has been studied. It is worth to mention to this end that this investigation is the first attempt to directly solve such governing partial differential equations for heat and mass transfer in the tridisperse porous media.

2 Basic equations

Consider the steady free convection in a two-dimensional porous square cavity. A schematic view of the physical model is shown in Fig. 1, where $\bar{x}$ and $\bar{y}$ are the Cartesian coordinates and L is the size of the cavity. It is assumed that the left vertical wall is heated and maintained at the constant temperature T_h, while the right vertical wall is cooled and has the constant temperature T_c. The horizontal walls are adiabatic $\frac{\partial T_f}{\partial y} = 0$, where T is the temperature.
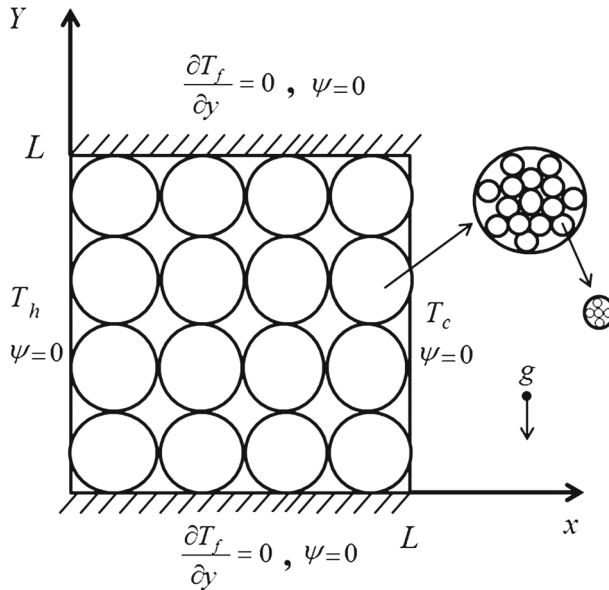
Fig. 1 Physical model and coordinate system

The application of TDPM could concern the nano-/micro-lattice meshes consisting of three levels of porosities. The micro-lattice fabricated by Rys et al. (2014) consists of three levels of porosities. The 3-phase of the micro-lattice of Rys et al. (2014) consists of nanometer size structures. The 3-phase of the nanolattices reported by Meza et al. (2014) consists of 10-nm ceramic nanostructures. For detailed thermal and hydraulic analysis of nano-/micro-lattices such as those reported in Rys et al. (2014) and Meza et al. (2014), a TDPM model is required that is subject of the present study. The porous matrices are assumed to be isotropic and homogenous throughout the enclosure. Apart from density variation in the buoyancy force which conforms to Boussinesq approximation, the other physical properties of the working fluid and the porous media are considered to be constant. It is considered that there is a local thermal equilibrium between the porous media and fluid in each scale. The conservation equations for the total mass, Darcy momentum, thermal energy come out to be as follows. A detailed derivation of these equations could be found in Nield and Kuznetsov (2011) and Kuznetsov and Nield (2011).

Continuum equations are:

$$\frac{\partial \overline{u}_1}{\partial x} + \frac{\partial \overline{v}_1}{\partial y} = 0, \tag{1a}$$

$$\frac{\partial \overline{u}_2}{\partial x} + \frac{\partial \overline{v}_2}{\partial y} = 0, \tag{1b}$$

$$\frac{\partial \overline{u}_3}{\partial x} + \frac{\partial \overline{v}_3}{\partial y} = 0. \tag{1c}$$

Momentum equations are:

$$\frac{\partial \overline{p}}{\partial \overline{x}} = -\frac{\mu}{K_1} \overline{u}_1 - \zeta_{12}(\overline{u}_1 - \overline{u}_2), \tag{2a}$$

$$\frac{\partial \overline{p}}{\partial \overline{x}} = -\frac{\mu}{K_2}\overline{u}_2 - \zeta_{12}(\overline{u}_2 - \overline{u}_1) - \zeta_{23}(\overline{u}_2 - \overline{u}_3), \tag{2b}$$

$$\frac{\partial \overline{p}}{\partial \overline{x}} = -\frac{\mu}{K_3}\overline{u}_3 - \zeta_{23}(\overline{u}_3 - \overline{u}_2), \tag{2c}$$

$$\frac{\partial \overline{p}}{\partial \overline{y}} = -\frac{\mu}{K_1}\overline{v}_1 - \zeta_{12}(\overline{v}_1 - \overline{v}_2) + \rho_F g\beta(T_F - T_\infty), \tag{3a}$$

$$\frac{\partial \overline{p}}{\partial \overline{y}} = -\frac{\mu}{K_2}\overline{v}_2 - \zeta_{12}(\overline{v}_2 - \overline{v}_1) - \zeta_{23}(\overline{v}_2 - \overline{v}_3) + \rho_F g\beta(T_F - T_\infty), \tag{3b}$$

$$\frac{\partial \overline{p}}{\partial \overline{y}} = -\frac{\mu}{K_3}\overline{v}_3 - \zeta_{23}(\overline{v}_3 - \overline{v}_2) + \rho_F g\beta(T_F - T_\infty), \tag{3c}$$

and the energy equations are:

$$\phi_1(\rho c)_1 \overline{V}_1 . \overline{\nabla} T_1 = \phi_1 k_1 \overline{\nabla}^2 T_1 + h_{12}(T_2 - T_1), \tag{4a}$$

$$(1 - \phi_1)\phi_2(\rho c)_2 \overline{V}_2 . \overline{\nabla} T_2 = (1 - \phi_1)\phi_2 k_2 \overline{\nabla}^2 T_2 + h_{12}(T_2 - T_1) + h_{23}(T_3 - T_2), \tag{4b}$$

$$(1 - \phi_1)(1 - \phi_2)(\rho c)_3 \overline{V}_3 . \overline{\nabla} T_3 = (1 - \phi_1)(1 - \phi_2)k_3 \overline{\nabla}^2 T_3 + h_{23}(T_2 - T_3), \tag{4c}$$

where the volume average of the temperature over the fluid is:

$$T_F = \frac{\phi_1 T_1 + (1 - \phi_1)\phi_2 T_2 + (1 - \phi_1)(1 - \phi_2)\phi_3 T_3}{\phi_1 + (1 - \phi_1)\phi_2 + (1 - \phi_1)(1 - \phi_2)\phi_3}, \tag{5}$$

We introduce now the following dimensionless variables as:

$$(\overline{x}, \overline{y}) = d(x, y) \quad \overline{p} = \frac{k_1\mu}{(\rho c)_1 K_1}p, \tag{6}$$

$$(\overline{u}_1, \overline{v}_1) = \frac{\phi_1 k_1}{(\rho c)_1 d}(u_1, v_1), \quad (\overline{u}_2, \overline{v}_2) = \frac{(1 - \phi_1)\phi_2 k_2}{(\rho c)_2 d}(u_2, v_2),$$

$$(\overline{u}_3, \overline{v}_3) = \frac{(1 - \phi_1)(1 - \phi_2)k_3}{(\rho c)_3 d}(u_3, v_3), \tag{7}$$

$$T_1 = (T_w - T_\infty)\theta_1 + T_\infty, \quad T_2 = (T_w - T_\infty)\theta_2 + T_\infty, \quad T_3 = (T_w - T_\infty)\theta_3 + T_\infty. \tag{8}$$

Also dimensionless parameters are:

$$\sigma_1 = \frac{\zeta_{12}K_1}{\mu}, \quad \sigma_2 = \frac{\zeta_{23}K_1}{\mu},$$

$$\beta_1 = \frac{(1 - \phi_1)\phi_2 k_2/(\rho c)_2}{\phi_1 k_1/(\rho c)_1}, \quad \beta_2 = \frac{(1 - \phi_1)(1 - \phi_2)k_3/(\rho c)_3}{\phi_1 k_1/(\rho c)_1}$$

$$K_{r1} = \frac{K_2}{K_1}, \quad K_{r2} = \frac{K_3}{K_1}, \tag{9}$$

Further, we introduced the stream function for three phases as:

$$u_1 = \frac{\partial \psi_1}{\partial y}, \, v_1 = -\frac{\partial \psi_1}{\partial x}$$

$$u_2 = \frac{\partial \psi_2}{\partial y}, \, v_2 = -\frac{\partial \psi_2}{\partial x}$$

$$u_3 = \frac{\partial \psi_3}{\partial y}, \, v_3 = -\frac{\partial \psi_3}{\partial x} \tag{10}$$

and Rayleigh number based on properties in 1-phase:

$$Ra = \frac{\rho_F g\beta(T_w - T_\infty)K_1 d}{\mu \phi_1 k_1/(\rho c)_1}. \tag{11}$$

Eliminating the pressure from Eqs. 2 and 3 and substituting Eqs. (6–10) in Eqs. (1–4) we have:

$$(1 + \sigma_1)\nabla^2 \psi_1 - \beta_1 \sigma_1 \nabla^2 \psi_2 = -Ra \frac{\partial \theta_F}{\partial x}, \tag{12a}$$

$$-\sigma_1 \nabla^2 \psi_1 + \beta_1 \left(\frac{1}{K_{r1}} + \sigma_1 + \sigma_2\right)\nabla^2 \psi_2 - \beta_2 \sigma_2 \nabla^2 \psi_3 = -Ra \frac{\partial \theta_F}{\partial x}, \tag{12b}$$

$$-\beta_1 \sigma_2 \nabla^2 \psi_2 + \beta_2 \left(\frac{1}{K_{r2}} + \sigma_2\right)\nabla^2 \psi_3 = -Ra \frac{\partial \theta_F}{\partial x}, \tag{12c}$$

and the thermal equations become:

$$\phi_1 \frac{\partial \psi_1}{\partial y}\frac{\partial \theta_1}{\partial x} - \phi_1 \frac{\partial \psi_1}{\partial x}\frac{\partial \theta_1}{\partial y} = \nabla^2 \theta_1 + H_1(\theta_2 - \theta_1), \tag{13a}$$

$$(1 - \phi_1)\phi_2 \frac{\partial \psi_2}{\partial y}\frac{\partial \theta_2}{\partial x} - (1 - \phi_1)\phi_2 \frac{\partial \psi_1}{\partial x}\frac{\partial \theta_1}{\partial y} = \nabla^2 \theta_2 + \gamma_1 H_1(\theta_1 - \theta_2) + \gamma_2 H_2(\theta_3 - \theta_2), \tag{13b}$$

$$(1 - \phi_1)(1 - \phi_2)\frac{\partial \psi_3}{\partial y}\frac{\partial \theta_3}{\partial x} - (1 - \phi_1)(1 - \phi_2)\frac{\partial \psi_3}{\partial x}\frac{\partial \theta_3}{\partial y} = \nabla^2 \theta_3 + \gamma_3 H_2(\theta_2 - \theta_3), \tag{13c}$$

where

$$\gamma_1 = \frac{\phi_1 k_1}{(1 - \phi_1)\phi_2 k_2}, \quad \gamma_2 = \frac{(1 - \phi_2)k_1}{\phi_2 k_2}, \quad \gamma_3 = \frac{k_1}{k_3}, \tag{14}$$

$$H_1 = \frac{h_{12}d^2}{\phi_1 k_1}, \quad H_2 = \frac{h_{23}d^2}{(1 - \phi_1)(1 - \phi_2)k_1}, \tag{15}$$

$$\theta_F = \frac{\phi_1 \theta_1 + (1 - \phi_1)\phi_2 \theta_2 + (1 - \phi_1)(1 - \phi_2)\phi_3 \theta_3}{\phi_1 + (1 - \phi_1)\phi_2 + (1 - \phi_1)(1 - \phi_2)\phi_3}, \tag{16}$$

and shorthand volume fractions are introduced as

$$\tau_1 = \frac{\phi_1}{\phi_1 + (1 - \phi_1)\phi_2 + (1 - \phi_1)(1 - \phi_2)\phi_3},$$

$$\tau_2 = \frac{(1 - \phi_1)\phi_2}{\phi_1 + (1 - \phi_1)\phi_2 + (1 - \phi_1)(1 - \phi_2)\phi_3}. \tag{17}$$

Using shorthand volume fraction (Eq. 17) Eqs. (12a–12c) become,

$$(1 + \sigma_1)\nabla^2\psi_1 - \beta_1\sigma_1\nabla^2\psi_2 = -Ra\left(\tau_1\frac{\partial\theta_1}{\partial x} + \tau_2\frac{\partial\theta_2}{\partial x} + (1 - \tau_1 - \tau_2)\frac{\partial\theta_3}{\partial x}\right), \tag{18a}$$

$$-\sigma_1\nabla^2\psi_1 + \beta_1\left(\frac{1}{K_{r1}} + \sigma_1 + \sigma_2\right)\nabla^2\psi_2 - \beta_2\sigma_2\nabla^2\psi_3$$

$$= -Ra\left(\tau_1\frac{\partial\theta_1}{\partial x} + \tau_2\frac{\partial\theta_2}{\partial x} + (1 - \tau_1 - \tau_2)\frac{\partial\theta_3}{\partial x}\right), \tag{18b}$$

$$-\beta_1\sigma_2\nabla^2\psi_2 + \beta_2\left(\frac{1}{K_{r2}} + \sigma_2\right)\nabla^2\psi_3 = -Ra\left(\tau_1\frac{\partial\theta_1}{\partial x} + \tau_2\frac{\partial\theta_2}{\partial x} + (1 - \tau_1 - \tau_2)\frac{\partial\theta_3}{\partial x}\right). \tag{18c}$$

The corresponding boundary conditions for these equations are given by,

$$\psi_1 = 0, \quad \psi_2 = 0, \quad \psi_3 = 0, \quad \theta_1 = 1, \quad \theta_2 = 1, \quad \theta_3 = 1 \text{ at } x = 0, \tag{19}$$

$$\psi_1 = 0, \quad \psi_2 = 0, \quad \psi_3 = 0, \quad \theta_1 = 0, \quad \theta_2 = 0, \quad \theta_3 = 0 \text{ at } x = 1, \tag{20}$$

$$\psi_1 = 0, \quad \psi_2 = 0, \quad \psi_3 = 0, \quad \frac{\partial\theta_1}{\partial y} = 0, \quad \frac{\partial\theta_2}{\partial y} = 0, \quad \frac{\partial\theta_3}{\partial y} = 0 \text{ at } y = 0 \text{ and } y = 1. \tag{21}$$

In addition, physical quantities of interest are the local Nusselt number Nu_1 of the 1-phase, Nu_2 of the 2-phase and Nu_3 of the 3-phase at the hot wall which are defined as follows,

$$Nu_1 = \frac{Lq_{w1}}{k_1(T_w - T_0)}, \quad Nu_2 = \frac{Lq_{w2}}{k_2(T_w - T_0)}, \quad Nu_3 = \frac{Lq_{w3}}{k_3(T_w - T_0)}, \tag{22}$$

here q_1, q_2 and q_3 are the heat fluxes of the 1-, 2- and 3-phases at the hot wall and are given by,

$$q_{w1} = -k_1\left(\frac{\partial T_1}{\partial x}\right)_{x=0}, \quad q_{w2} = -k_2\left(\frac{\partial T_2}{\partial x}\right)_{x=0}, \quad q_{w3} = -k_3\left(\frac{\partial T_3}{\partial x}\right)_{x=0}. \tag{23}$$

Applying dimensionless variables (Eq. 8), we obtain from Eqs. 22 and 23,

$$Nu_1 = -\left(\frac{\partial\theta_1}{\partial x}\right)_{x=0}, \quad Nu_2 = -\left(\frac{\partial\theta_2}{\partial x}\right)_{x=0}, \quad Nu_3 = -\left(\frac{\partial\theta_3}{\partial x}\right)_{x=0}. \tag{24}$$

It is worth noting that, despite previous investigations, in this study the parameters H_1, H_2, associated with dimensionless inter-phase heat transfer and γ_1, γ_2 and γ_3 denoting the modified thermal conductivity ratios are considered in Eqs. (13a–c).

3 Numerical method and validation

The set of partial differential equations (Eqs. 13 and 18) subject to the boundary conditions Eqs. 19, 20, 21 has been solved employing finite element method. Utilizing Galerkin finite element method (Reddy 1993), the set of governing partial differential equations transformed to the weak form and solved numerically. A nonuniformed mesh is utilized. The mesh points are clustered near the walls to increase the accuracy of the solution and capture gradients near the walls. A view of the utilized mesh structure of size 25×25 with the element ratio 20 is depicted in Fig. 2. This size of the mesh is selected to clearly illustrate the mesh structure. As seen, the mesh points are clustered near the walls. The largest element size is in the

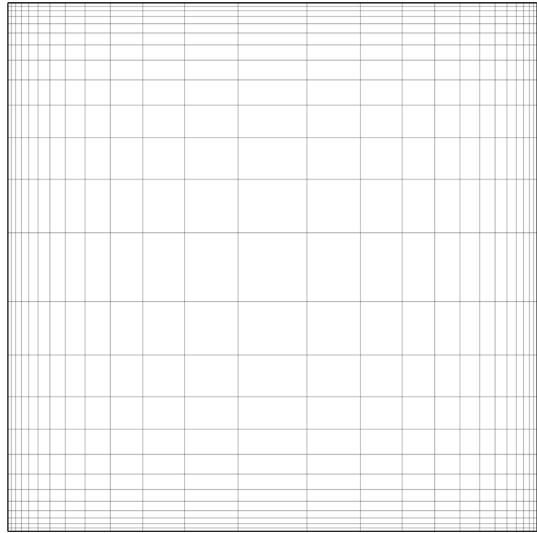**Fig. 2** A view of the utilized mesh with the size of 25 × 25 and the element ratio 20

Table 1 Grid check by evaluated Nusselt number in different *Ra* for regular porous medium using a uniform grid

Ra	Grid size					
	50 × 50	100 × 100	200 × 200	230 × 230	300 × 300	400 × 400
10	1.0800	1.0791	1.0791	1.0800	1.0791	1.0791
100	3.1144	3.1121	3.1115	3.1115	3.1114	3.1114
1000	14.1740	13.6490	13.6550	13.6660	13.6730	13.7950
10,000	66.5830	56.6330	51.4370	50.9280	50.6300	49.6040

middle of the cavity with the nondimensional size of 0.13, while the smallest element sizes are in the corners with the size of 0.0065. The Lagrange shape functions with quadratic shape functions are utilized for discretization of the momentum equations. A linear discretization is utilized for heat equations. Fourth-order elements are utilized for calculation of the fluxes at the walls. A fourth-order integration based on the Gaussian quadrature is also utilized to calculate the heat flux (Nusselt number) at the boundaries.

Moreover, the Newton–Raphson method was applied to solve the discretized equations. The detailed solution can be found in the previous studies (Reddy 1993; Basak et al. 2006). The iteration process terminates when the changes in the dependent variables between two subsequent iterations are satisfied by establishing the following criterion:

$$\frac{\sum \left| \kappa_{i,j}^{n+1} - \kappa_{i,j}^{n} \right|}{\sum \left| \kappa_{i,j}^{n+1} \right|} \leq 10^{-8}, \tag{25}$$

here $\kappa_{i,j}^{n}$ denotes the dependent variables at iteration n.

Tables 1 and 2 show the evaluated mean Nusselt numbers of regular porous medium for different grid sizes. Table 1 shows the results for a regular uniform grid, and Table 2 shows the results for a nonuniform grid clustered near the walls. Table 2 demonstrates that the grid

Table 2 Grid check by evaluated Nusselt number in different *Ra* for regular porous medium using a nonuniform grid and element ratio 20

Ra	Grid size					
	50×50	100×100	200×200	230×230	300×300	400×400
10	1.0800	1.0791	1.0791	1.0800	1.0791	1.0791
100	3.1121	3.1115	3.1114	3.1114	3.1114	3.1114
1000	13.6540	13.6440	13.6420	13.6420	13.6410	13.6410
10,000	49.7950	48.8480	48.5700	48.5540	48.5280	48.5100

Table 3 Comparison of Nusselt number calculated using the nonuniform grid (230×230 grid points and element ratio 20) with the results from the open literature

Authors	Ra			
	10	100	1000	10,000
Bejan (1979)		4.200	15.800	50.8
Beckermann et al. (1986)		3.113		48.9
Gross et al. (1986)		3.141	13.448	42.583
Moya et al. (1987)	1.065	2.801		
Manole and Lage (1992)		3.118	13.637	48.117
Baytas and Pop (1999)	1.079	3.160	14.060	48.330
Sheremet and Pop (2014b)	1.071	3.104	13.839	49.253
Present results	1.080	3.111	13.642	48.554

size of 230×230 with element ratio 20 provides accurate results within almost two digits of accuracy for Nusselt number expect for the case of $Ra = 10{,}000$. Since all results of this paper are at $Ra = 1000$, all of the calculations have been executed using the grid size of 230×230.

In the first validation of the present study, neglecting the effect of tridisperse porous medium by setting the parameters as ($\phi_1 = 1$, $\phi_{2,3} = H_{1,2} = \sigma_{1,2} = 0$) and considering steady-state problem, is reduced to the study of a regular porous medium (monodisperse porous medium) saturated with a pure fluid which was analyzed by several investigators. In this case, a comparison between the computed value of the Nusselt number and those given by multifarious authors from open literature is performed in Table 3.

Figure 3 also shows another validation of the average Nusselt number at the hot wall setting the parameters: $\tau_1 = 0.625$, $\tau_2 = 0.375$, $\sigma_1 = 1$, $\sigma_2 = 0$, $K_1 = 0.1$, $K_2 = 0.0001$, $K_{r1} = 0.001$, $K_{r2} = 0^+$ (in which $0^+ = 10^{-15}$), $Ra = 1000$, $\beta_1 = 10$, $\beta_2 = 0^+$, $\gamma_1 = 1$, $\gamma_2 = 0$, $\gamma_3 = 0$, $\phi_1 = 0.5$, $\phi_2 = 0.6$, $\phi_3 = 0$, and considering the applied difference temperature to be $1°$. Comparing the results with the data reported by Revnic et al. (2009), it is obvious that there is a good agreement between the results of the present study and the previous ones.

4 Results and discussion

The governing equations (Eqs. 13 and 18) consist of sixteen parameters that can be adjusted and investigated the effect of each one on the fluid flow and heat transfer, but in this paper according to other similar studies we set constant some parameters and check the effect of the other ones. The magnitude of the governing parameters is set as follows: fluid volume
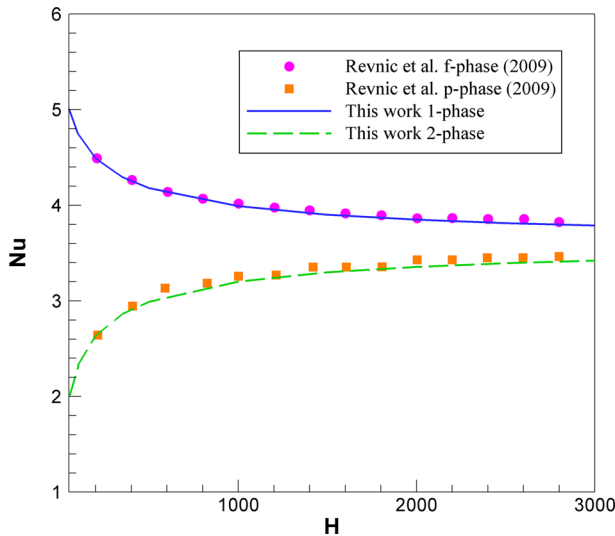
Fig. 3 Comparison of the average Nusselt number of the hot wall for BDPM between this work and Revnic et al. (2009)

fraction $\phi = 0.4$ so that $\tau_1 = 0.510$ and $\tau_2 = 0.306$, modified thermal conductivity ratio $\gamma = 1$, modified thermal diffusivity ratio $\beta = 10$, inter-phase momentum transfer $\sigma = 1$, permeability ratio $K_r = 0.001$, dimensionless inter-phase heat transfer parameter $H = 50$, the Raleigh number $Ra = 1000$ and the applied difference temperature is 1 degree where $\phi_1 = \phi_2 = \phi_3 = \phi$, $\beta_1 = \beta_2 = \beta$, $\gamma_1 = \gamma_2 = \gamma_3 = \gamma$, $\sigma_1 = \sigma_2 = \sigma$, $K_{r1} = K_r$, $K_{r2} = K_r^2$, $H_1 = H_2 = H$ similar to the Revnic et al. (2009) and Nield and Kuznetsov (2011) which we call these above values the base condition. It is worth mentioning that, except the specific parameter that would be investigated, we adopt the above-mentioned values constant.

The results for the flow and temperature fields are represented with streamlines and isothermal contours of 1-, 2- and 3-phases for the base parameters in Fig. 4. As it can be seen, the streamline contours for three phases have the same shape as it is shown by Revnic et al. (2009) for BDPM, but the temperature fields are different in three phases.

The effect of different parameters on the heat transfer is shown in Figs. 5, 6, 7, 8 and 9. Figure 5 shows the Nusselt number for three phases at different values of β. The results show that decreasing β from 100 to 0.1 does not have a significant impact on the amount of Nusselt numbers. Moreover, it is shown that increasing dimensionless inter-phase heat transfer parameter (H) leads to decrease in 1-phase Nusselt number and increase in 2-phase and 3-phase Nusselt numbers. In addition, it could be seen that when the value of parameter H is high, the further increase of H does not show any noticeable influence on the heat transfer.

The effect of permeability ratio K_r on the Nusselt number at wide range of inter-phase heat transfer parameter H is depicted in Fig. 6. In accordance with Fig. 6, by increasing K_r from 0.001 to 1, the values of Nusselt numbers for three phases increase. Furthermore, it seems that rate of convergence of Nusselt numbers of 2-phase and 3-phase in high values of parameter H is altered by variation of permeability ratio. Figure 7 illustrates the variation of Nusselt number for different inter-phase momentum transfer parameter σ. It is shown that the heat flux increases as σ dwindles from 1 to 0.0001
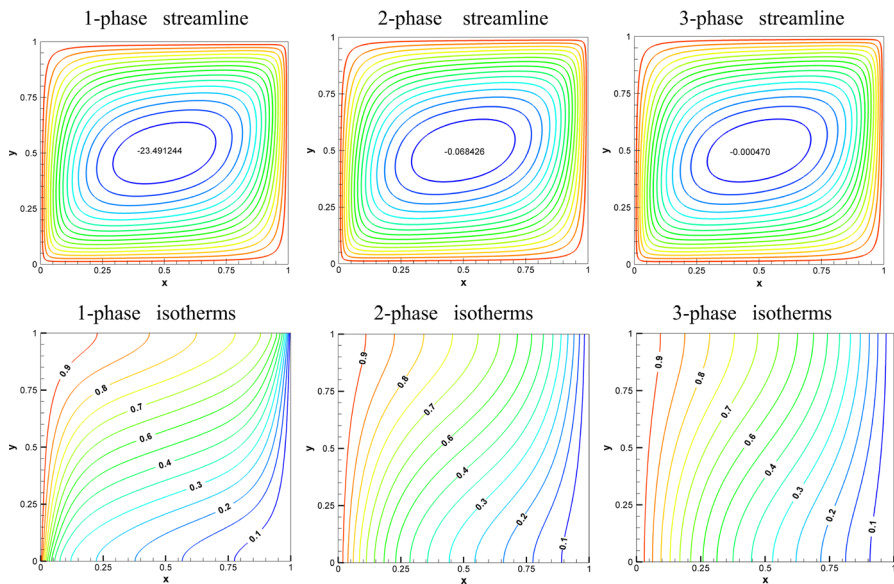
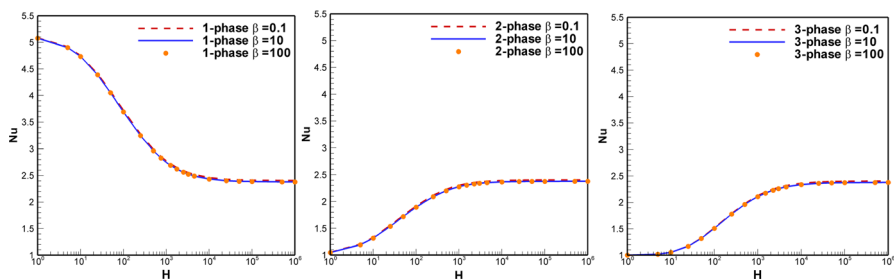**Fig. 4** Streamlines and isotherm contours for the default combination of parameters
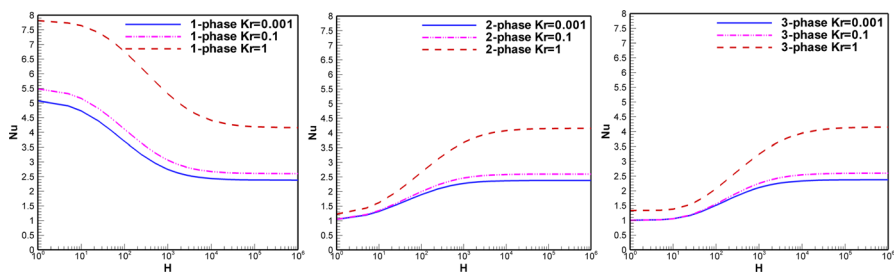

Fig. 5 Nusselt number as a function of β

Fig. 6 Nusselt number as a function of K_r

Figure 8 presents the effect of variation of modified thermal conductivity ratio, i.e., γ, on the Nusselt number. According to Fig. 8, the Nusselt number is an increasing function of the parameter γ. Moreover, as it is shown, for small magnitudes of γ, i.e., $\gamma = 0.01$, increasing H above 1000 does not have significant effect on the heat transfer and the Nusselt numbers have almost the same value for three phases.
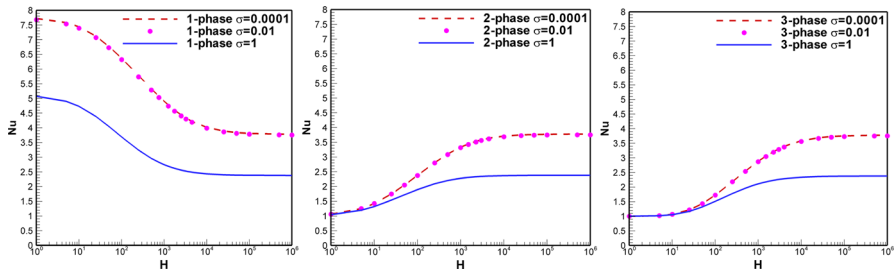
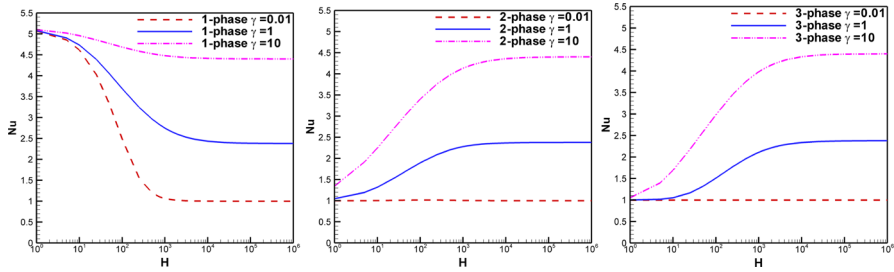**Fig. 7** Nusselt number as a function of σ
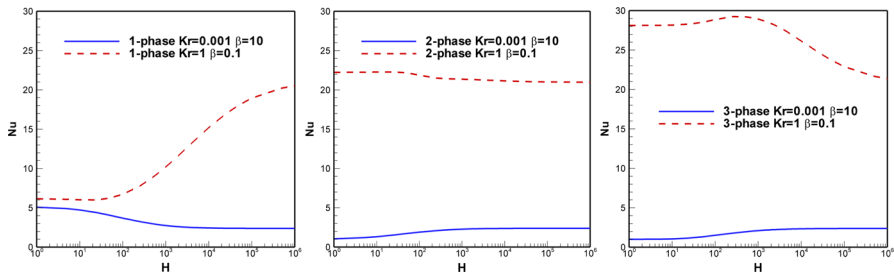

Fig. 8 Nusselt number as a function of γ

Fig. 9 Nusselt number as a function of K_r and β

Figure 9 shows an exception condition so that when K_r is high value and β is low, independent of the value of σ, the Nusselt number values of 2- and 3-phases are more than 1-phase. This fact is also shown in Table 4 (see cases 3, 12 and 21). For instance, in case 3, $Nu_3 > Nu_2 > Nu_1$ with the values 28.52282, 22.18428 and 6.248895, respectively. Moreover, in this condition, the value of Nusselt numbers of three phases has significant difference with each other compared to the other conditions.

5 Conclusion

Considering the Darcy model, an internal natural convection in a square cavity filled with tridisperse porous medium under steady-state condition has been studied. It is assumed that the porous matrices are isotropic and homogenous throughout the enclosure. Furthermore, the horizontal and vertical boundaries are assumed to be constant temperature and adiabatic, respectively. The effect of governing parameters such as modified thermal conductivity ratio γ, modified thermal diffusivity ratio β, inter-phase momentum transfer parameter σ, perme-

Table 4 Numerical results of base condition for different values of σ, β, K_{r1}

Case	σ	B	K_{r1}	$-\theta_{1x}$	$-\theta_{2x}$	$-\theta_{3X}$
1	0.0001	0.1	0.0001	6.779025	2.056071	1.435738
2	0.0001	0.1	0.01	6.942712	2.214437	1.485519
3	0.0001	0.1	1	6.248895	22.18428	28.52282
4	0.0001	1	0.0001	6.77749	2.054835	1.435339
5	0.0001	1	0.01	6.794532	2.068695	1.439944
6	0.0001	1	1	7.81639	5.658928	7.214223
7	0.0001	10	0.0001	6.777337	2.054711	1.435299
8	0.0001	10	0.01	6.779051	2.056077	1.435755
9	0.0001	10	1	7.127155	2.309401	1.771319
10	0.01	0.1	0.0001	6.732038	2.051333	1.434187
11	0.01	0.1	0.01	6.897831	2.211975	1.484711
12	0.01	0.1	1	6.248895	22.18428	28.52282
13	0.01	1	0.0001	6.730486	2.05008	1.433781
14	0.01	1	0.01	6.748181	2.064165	1.438466
15	0.01	1	1	7.81639	5.658928	7.214223
16	0.01	10	0.0001	6.730331	2.049955	1.433741
17	0.01	10	0.01	6.732534	2.051387	1.434219
18	0.01	10	1	7.127155	2.309401	1.771319
19	1	0.1	0.0001	4.050102	1.720922	1.31881
20	1	0.1	0.01	4.341496	2.026506	1.421906
21	1	0.1	1	6.248895	22.18428	28.52282
22	1	1	0.0001	4.047649	1.718753	1.318014
23	1	1	0.01	4.120125	1.749857	1.329533
24	1	1	1	7.81639	5.658928	7.214223
25	1	10	0.0001	4.047404	1.718537	1.317934
26	1	10	0.01	4.095945	1.727847	1.321396
27	1	10	1	7.127155	2.309401	1.771319

ability ratio K_r and dimensionless inter-phase heat transfer parameter H on three phases of porosity for TDPM cavity has been numerically studied. As it is seen, apart from the exceptional case which is discussed in Fig. 8, when the value of H is high, there is no noticeable difference between Nusselt numbers of three phases of porosity and in all reviewed cases there is no significant difference for Nusselt value between 2- and 3-phases. In addition, the Nusselt numbers are an increasing function of γ and K_r and a decreasing function of σ.

References

Basak, T., Roy, S., Paul, T., Pop, I.: Natural convection in a square cavity filled with a porous medium: effects of various thermal boundary conditions. Int. J. Heat Mass Transf. **49**, 1430–1441 (2006)

Baytas, A.C., Pop, I.: Free convection in oblique enclosures filled with a porous medium. Int. J. Heat Mass Transf. **42**, 1047–1057 (1999)

Baytas, A.C., Pop, I.: Natural convection in a trapezoidal enclosure filled with a porous medium. Int. J. Eng. Sci. **39**, 125–134 (2001)

Beckermann, C., Viskanta, R., Ramadhyani, S.: A numerical study of non-Darcian natural convection in a vertical enclosure filled with a porous medium. Numer. Heat Transf. **10**, 446–469 (1986)

Bejan, A.: On the boundary layer regime in a vertical enclosure filled with a porous medium. Lett. Heat Mass Transf. **6**, 93–102 (1979)

Bejan, A., Dincer, I., Lorente, S., Miguel, A.F., Reis, A.H.: Porous and Complex Flow Structures in Modern Technologies. Springer, New York (2004)

Chen, Z.Q., Cheng, P., Hsu, C.T.: A theoretical and experimental study on stagnant thermal conductivity of bi-dispersed porous media. Int. Commun. Heat Mass Transf. **27**, 601–610 (2000a)

Chen, Z.Q., Cheng, P., Zhao, T.S.: An experimental study of two phase flow and boiling heat transfer in bi-disperse porous channels. Int. Commun. Heat Mass Transf. **27**, 293–302 (2000b)

Cheng, C.Y.: Natural convection heat transfer about a vertical cone embedded in a tridisperse porous medium. Transp. Porous Media **107**, 765–779 (2015)

De Lemos, M.J.S.: Turbulence in Porous Media: Modeling and Applications, 2nd edn. Elsevier, Oxford (2012)

Ghalambaz, M., Sheremet, M.A., Pop, I.: Free convection in a parallelogrammic porous cavity filled with a nanofluid using Tiwari and Das' nanofluid model. PLOSE ONE. 17/17 (2015). doi:10.1371/journal.pone.0126486

Gross, R., Bear, M.R., Hickox, C.E.: The application of flux-corrected transport (FCT) to high Rayleigh number natural convection in a porous medium. In: Proceedings of the 7th International Heat Transfer Conference, San Francisco, CA (1986)

Ingham, D.B., Pop, I. (eds.): Transport Phenomena in Porous Media. Elsevier, Oxford (2005)

Kuznetsov, A.V., Nield, D.A.: The onset of convection in a tridisperse porous medium. Int. J. Heat Mass Transf. **54**, 3120–3127 (2011)

Manole, D.M., Lage, J.L.: Numerical benchmark results for natural convection in a porous medium cavity. Heat Mass Transf. Porous Media ASME Conf. **105**, 44–59 (1992)

Meza, L.R., Das, S., Greer, J.R.: Strong, lightweight, and recoverable three-dimensional ceramic nanolattices. Science **345**(6202), 1322–1326 (2014)

Moya, S.L., Ramos, E., Sen, M.: Numerical study of natural convection in a tilted rectangular porous material. Int. J. Heat Mass Transf. **30**, 630–645 (1987)

Nield, D.A., Bejan, A.: Convection in Porous Media, 4th edn. Springer, New York (2013)

Nield, D.A., Kuznetsov, A.V.: Forced convection in a bi-disperse porous medium channel: a conjugate problem. Int. J. Heat Mass Transf. **47**, 5375–5380 (2004)

Nield, D.A., Kuznetsov, A.V.: The Cheng–Minkowycz problem for natural convection about a vertical plate embedded in a tridisperse porous medium. Int. J. Heat Mass Transf. **54**, 3485–3493 (2011a)

Nield, D.A., Kuznetsov, A.V.: A three-velocity three-temperature model for a tridisperse porous medium: forced convection in a channel. Int. J. Heat Mass Transf. **54**, 2490–2498 (2011b)

Nield, D.A., Kuznetsov, A.V.: The effect of vertical throughflow on thermal instability in a porous medium layer saturated by a nanofluid: a revised model. ASME J. Heat Transf. **137**, 052601-1–052601-5 (2015)

Pop, I., Ingham, D.B.: Convective Heat Transfer: Mathematical and Computational Modeling of Viscous Fluids and Porous Media. Pergamon, Oxford (2001)

Reddy, J.N.: An Introduction to the Finite Element Method. McGraw-Hill, New York (1993)

Revnic, C., Grosan, T., Pop, I., Ingham, D.B.: Free convection in a square cavity filled with a bidisperse porous medium. Int. J. Therm. Sci. **48**, 1876–1883 (2009)

Rys, J., Valdevit, L., Schaedler, T.A., Jacobsen, A.J., Carter, W.B., Greer, J.R.: Fabrication and deformation of metallic glass micro-lattices. Adv. Eng. Mater. **16**(7), 889–896 (2014)

Sheremet, M.A., Pop, I.: Thermo-bioconvection in a square porous cavity filled by oxytactic microorganisms. Transp. Porous Media **103**, 191–205 (2014a)

Sheremet, M.A., Pop, I.: Natural convection in a square porous cavity with sinusoidal temperature distributions on both side walls filled with a nanofluid: Buongiorno's mathematical model. Transp. Porous Media **105**, 411–429 (2014b)

Sheremet, M.A., Grosan, Pop, I.: Free convection in a square cavity filled with a porous medium saturated by nanofluid using Tiwari and Das' nanofluid model. Transp. Porous Media **106**, 595–610 (2015)

Vadasz, P. (ed.): Emerging Topics in Heat and Mass Transfer in Porous Media. Springer, New York (2008)

Vafai, K. (ed.): Handbook of Porous Media, 2nd edn. Taylor & Francis, New York (2005)